Available online at www.sciencedirect.com
ScienceDirect
Trans. Nonferrous Met. Soc. China 32(2022) 3197−3211
Transactions of Nonferrous Metals Society of China
www.tnmsc.cn

Improvement of high-temperature strength of 6061 Al matrix composite reinforced by dual-phased nano-AlN and submicron-Al_2O_3 particles

Ke-wei XIE[1], Jin-feng NIE[2], Kai-qi HU[1], Xia MA[3], Xiang-fa LIU[1]

1. Key Laboratory for Liquid–Solid Structural Evolution & Processing of Materials, Ministry of Education, Shandong University, Jinan 250061, China;
2. Nano and Heterogeneous Materials Center, School of Materials Science and Engineering, Nanjing University of Science and Technology, Nanjing 210094, China;
3. School of Mechanical Engineering, Shandong University of Technology, Zibo 255000, China

Received 29 August 2021; accepted 9 March 2022

Abstract: Nano-AlN and submicron-Al_2O_3 particles were simultaneously utilized in a 6061 Al matrix composite to improve the high-temperature strength. According to the SEM and TEM characterization, nano-AlN and submicron-Al_2O_3 particles are uniformly distributed in the Al matrix. Brinell hardness results indicate that different from the traditional 6061 Al matrix alloy, the aging kinetics of the composite is obviously accelerated by the reinforcement particles. The T6-treated composite exhibits excellent tensile properties at both room temperature and elevated temperature. Especially at 350 °C, the T6-treated composite not only has a high yield strength of 121 MPa and ultimate tensile strength of 128 MPa, but also exhibits a large elongation of 11.6%. Different strengthening mechanisms of nano-AlN and submicron-Al_2O_3 particles were also discussed in detail.

Key words: 6061 Al matrix composite; nano-AlN particles; submicron-Al_2O_3 particles; high-temperature strength

1 Introduction

Particle-reinforced aluminum matrix composites with high specific strength, high stiffness and good wear resistance have received increasing attention in the fields of automobile, aerospace, etc. [1−3]. In order to satisfy higher requirements on energy conservation and emission reduction, it is urgent to further enhance the high-temperature mechanical properties and thermal stability of aluminum alloys and aluminum matrix composites [4,5]. Generally, precipitation hardening is considered to be one of the most important strengthening mechanisms for Al−Cu and Al− Mg−Si matrix alloys [6−8]. 6061 Al alloy, as a typical Al−Mg−Si alloy, has been widely applied in airframe, ship, appliances, due to its medium strength, excellent formability and weldability, good corrosion resistance and low cost [9−12]. Generally, the room temperature mechanical properties can be enhanced significantly due to the nano-sized precipitates [13,14]. However, owing to coarsening, phase transformation and/or dissolution at elevated working temperature higher than 200 °C, these precipitates would lose their strengthening effect and then lead to severe deterioration in mechanical properties, as reported in Refs. [15−17].

Compared with these precipitates in Al alloys, most ceramic reinforcement particles have sufficient stability at high temperatures. Thus, one sensible approach is by utilizing the thermally

Corresponding author: Jin-feng NIE, Tel: +86-531-88392006, Fax: +86-531-88395414, E-mail: niejinfeng@njust.edu.cn; Xiang-fa LIU, E-mail: xfliu@sdu.edu.cn
DOI: 10.1016/S1003-6326(22)66013-8

stable ceramic particles to strengthen the Al matrix and make up for the deteriorated properties at elevated temperatures [18−20]. Among the ceramic particles, AlN and Al_2O_3 as reinforcement have obvious advantages because of their high melting point (AlN: 2200 °C; Al_2O_3: 2030 °C), high elastic modulus (AlN: 310 GPa; Al_2O_3: 379 GPa) and other excellent properties [19,21]. According to our previous study [22], most nano-AlN particles are easily agglomerated in a small scale, which limits the ductility of the composite to a large extent. In order to improve the ductility, heat-resistant Al composites reinforced by dual-phased nano-AlN and submicron-Al_2O_3 have been fabricated using liquid−solid reaction method. Interestingly, the agglomerated nano-AlN particles distribute more uniformly in Al matrix due to the addition of submicron-Al_2O_3 particles. It is shown that the $(8.2\ AlN + 1\ Al_2O_3)_p$/Al (mass fraction, %) composite has the optimum ductility with an increased tensile strength. Moreover, there is robust interfacial bonding between the reinforcement particles (AlN and Al_2O_3) and Al matrix, which is considered to be one of the main reasons for excellent mechanical properties. However, to the best of our knowledge, the influence of the dual-phased and bimodal-sized particles, i.e., the in-situ nano-AlN particles and ex-situ submicron-Al_2O_3 particles, on the microstructure and mechanical properties of 6061 Al matrix composites has not been reported. In addition, the intrinsic influence mechanism is still unclear, which needs to be further studied.

Motivated by the above considerations, in the present work, we fabricated $(8.2\ AlN + 1\ Al_2O_3)_p$/6061 Al composite to further enhance the high-temperature strength of 6061 Al alloy. The effects of dual-phased nano-AlN and submicron-Al_2O_3 particles on the age hardening behavior, microstructure, mechanical properties at room temperature and 350 °C, and the strengthening mechanisms of the composite were discussed. Our work may provide some guidance for the application of popular 6061 Al alloys under an elevated temperature service condition.

2 Experimental

2.1 Materials preparation

The raw materials used in this work include commercial 6061 Al powders (actual chemical compositions of Al−1%Mg−0.6%Si−0.3%Cu (all compositions quoted in this work are nominal values in mass fractions unless otherwise stated) detected by spectrum, with average diameter of ~50 μm) with the purity of 99.7%, nitride plastid powders (average diameter of ~2 μm) with the purity of 98.5% and hexagonal α-Al_2O_3 particles (average diameter of ~0.45 μm) with the purity of 99.9%, as reported in our previous work [22]. The 6061 Al matrix composite with 8.2% AlN and 1% Al_2O_3 particles ($(8.2\ AlN + 1\ Al_2O_3)_p$/6061) was fabricated in the vacuum furnace (SRYL−1400H, SIOMM) under argon gas protection, and after liquid−solid reaction, the obtained ingots were extruded by the extrusion press (JS−650T) at 500 °C with an extrusion ratio of ~16:1. Subsequently, the solid solution and aging treatments were employed to further enhance the mechanical properties. In addition, the unreinforced 6061 Al alloy was prepared according to the same processing parameters for comparison. The whole experimental procedure is revealed in Fig. 1.

Samples were solution-treated at 550 °C for 2 h, then water-quenched and aged at 175 °C for different time in order to determine the optimal aging treatment.

2.2 Mechanical test

Brinell hardnesses of the 6061 Al matrix alloy and the $(8.2\ AlN + 1\ Al_2O_3)_p$/6061 Al composite before and after aging were measured by the digital Brinell hardness tester (HBST−3000AET, Laishi) according to the ASTM E10—14 Standard. The diameter of the indenter was 5 mm, and the load was 2452 N (250 kgf) with a dwell time of 60 s. In each case, at least six positions were tested to obtain an average value. To verify the strengthening effects of AlN and Al_2O_3 particles on the matrix, tensile tests were carried out at room and elevated temperature (350 °C), respectively. The tensile test samples were cut from the extrusion rod and processed into dog-bone shaped tensile test bars. The specimens of tensile test bar at room temperature has a gauge cross-section of 5 mm in diameter and 25 mm in original gauge length, and the specimens of tensile test bar at 350 °C have a gauge cross section of 10 mm in diameter and 50 mm in original gauge length. All the tensile bars were tested on the electromechanical universal testing machine (WDW−100D) at a loading rate of

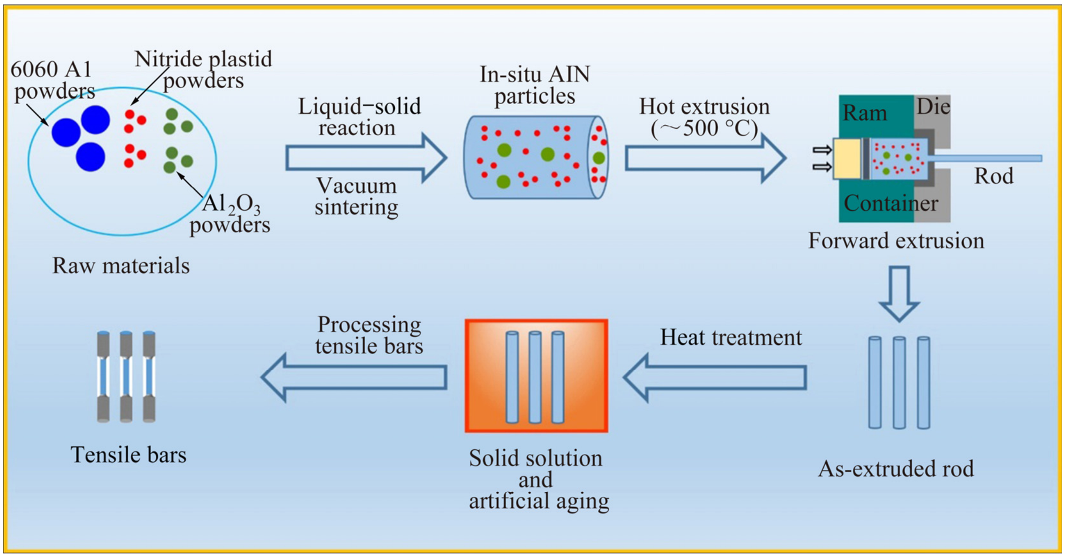

Fig. 1 Schematic diagram of experimental procedure for $(8.2\ AlN + 1\ Al_2O_3)_p$/6061 Al composite, involving liquid−solid reaction, hot extrusion, and heat treatment process (The 6061 Al matrix alloy was also prepared by similar processes for comparison)

2 mm/min. Before the elevated temperature tensile test, the specimens were heated to the specified temperature and then held for at least 30 min. To make sure the accuracy of measurement, each sample was tested at least three times and then the average value was taken.

2.3 Microstructure characterization

The phase compositions and microstructures of the composites were characterized by field emission scanning electron microscope (FE-SEM, JSM−7800F, Japan) equipped with an energy dispersive X-ray spectroscope (EDS, XMax−80) detector. The crystallographic orientation, grain size and geometrically necessary dislocation (GND) density evaluation were investigated through electron backscattered diffraction (EBSD) technique and analyzed by Channel 5 software. And samples for EBSD analysis were prepared by Ar ion milling using a cross section polisher (CP; JEOL, IB−19510CP) at 6 kV for 3 h. Data collection was also performed on the JSM−7800F microscope linked with NordlysMax3 detector at an accelerating voltage of 20 kV. A TECNAI G2 200 high resolution transmission electron microscope (TEM) with a spherical aberration corrector under the objective lens operated at 300 kV was used to analyze the reinforcement particles and dislocations in the matrix. Samples for TEM observation were ground to 60 μm firstly, and then punched into thin slices with a diameter of 3 mm. Then, the slices were polished by ion beam thinning (Gatan 695) at an acceleration voltage of 5 kV and a beam angle of ~7° for perforation, and at an acceleration voltage of 3 kV and a beam angle of ~4° for final trimming.

3 Results

3.1 Age hardening behavior of $(8.2\ AlN+1\ Al_2O_3)_p$/6061 Al composite

In order to evaluate the strengthening effect of AlN and Al_2O_3 particles, Brinell hardness tests were conducted for $(8.2\ AlN + 1\ Al_2O_3)_p$/6061 Al composite and 6061 alloy at room temperature, as shown in Fig. 2. It can be seen that the hardness of the as-cast composite is 55.8% higher than that of the 6061 matrix alloy. After the hot extrusion, the hardness is increased by 85.8% due to the significant grain refinement during the extrusion process. In addition, the hardness of the composite is further enhanced by 38.0% after solution treatment (as-quenched condition). Thus, it can be seen that the hardness of the composite is considerably increased by the AlN and Al_2O_3 particles.

Figure 3 shows the age hardening curves of 6061 matrix alloy and $(8.2\ AlN + 1\ Al_2O_3)_p$/6061 Al composite at 175 °C for different holding time after solution treatment at 550 °C for 2 h. It can be seen that the hardness is firstly increased with prolonged

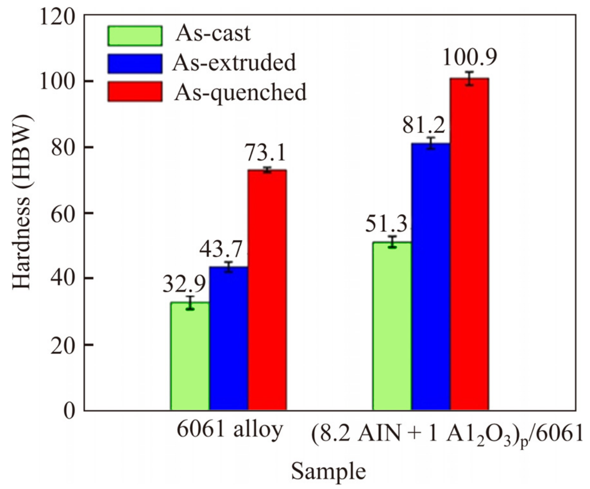

Fig. 2 Brinell hardness of 6061 alloy and (8.2 AlN + 1 $Al_2O_3)_p$/6061 Al composite (as-cast, as-extruded and as-quenched conditions, respectively)

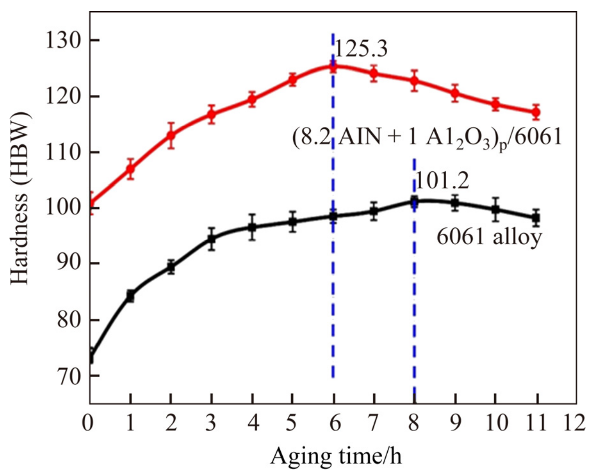

Fig. 3 Variation of Brinell hardness versus aging time of 6061 alloy and (8.2 AlN + 1 $Al_2O_3)_p$/6061 Al composite aged at 175 °C after solution treatment at 550 °C for 2 h

aging time, and then reaches the peak aging. The hardnesses of (8.2 AlN + 1 $Al_2O_3)_p$/6061 Al composite and 6061 alloy are increased by 24.2% (from HBW 100.9 to HBW 125.3) and by 38.4% (from HBW 73.1 to HBW 101.2), respectively. Moreover, it is noticed that the time for the composite to reach the peak aging (6 h) is shorter than that of the 6061 matrix alloy (8 h), suggesting that the aging kinetics of the composite is accelerated by the AlN and Al_2O_3 particles, which is helpful to shorten the heat treatment time and improve production efficiency in practice. To summarize, the optimized aging treatment of (8.2 AlN + 1 $Al_2O_3)_p$/6061 Al composite is measured to be at 175 °C for 6 h.

3.2 Microstructure of (8.2 AlN + 1 $Al_2O_3)_p$/6061 Al composite

Figure 4 presents the microstructures of T6-treated (8.2 AlN + 1 $Al_2O_3)_p$/6061 Al composite. It can be seen that lots of reinforcement particles are uniformly distributed in the matrix (Figs. 4(a) and (b)). According to the EDS results given in Figs. 4(e) and (f), the white particles in the matrix with size smaller than 1 μm are Al_2O_3 and most of the nano-sized particles smaller than 100 nm are AlN, as labeled by the yellow arrows and circle in Fig. 4(c), respectively. It also shows that nano-AlN particles and submicron-Al_2O_3 particles have regular morphologies in Figs. 4(c) and (d). Meanwhile, it is supposed that the uniform distribution of dense AlN and Al_2O_3 particles will lead to a high strength of the composite. Furthermore, Figs. 5(a) and (b) present statistical size distribution for the reinforcement particles, and the average sizes are measured to be ~50 nm for AlN and ~0.45 μm for Al_2O_3, respectively.

Figure 6 shows the typical TEM images of the T6-treated (8.2 AlN + 1 $Al_2O_3)_p$/6061 Al composite. As indicated by red arrows in Fig. 6(a), nano-AlN particles are distributed both at the grain boundaries and in the interior of α(Al) grains. Meanwhile, the white Al_2O_3 particles are also detected in the matrix (marked by green arrows). Furthermore, a higher magnification of Fig. 6(b) shows that a large number of nano-sized AlN particles are distributed in the matrix, indicating a fine intragranular dispersion. It is noteworthy that lots of dislocations can be found in the α(Al) grains indicated by yellow arrows in Fig. 6(c), suggesting the effective accumulation of dislocations in the matrix. What's more, the dislocations in the composite show a more complex and tangled feature owing to the interactions with the nano-AlN particles both at the grain boundaries and in the interior of α(Al) grains (indicated by yellow arrows in Fig. 6(d)). In addition, from all the micrographs, no voids and cracks can be seen, which indicates the robust bonding between the matrix and the reinforcement particles. For the composites, such a strong bonding between the matrix and the particles is the key factor for the enhanced mechanical performance.

The preferred orientation distributions of α(Al) grains in the 6061 alloy and (8.2 AlN + 1 $Al_2O_3)_p$/6061 Al composite were also detected, Fig. 7 depicts the EBSD analyses of α(Al) grains along

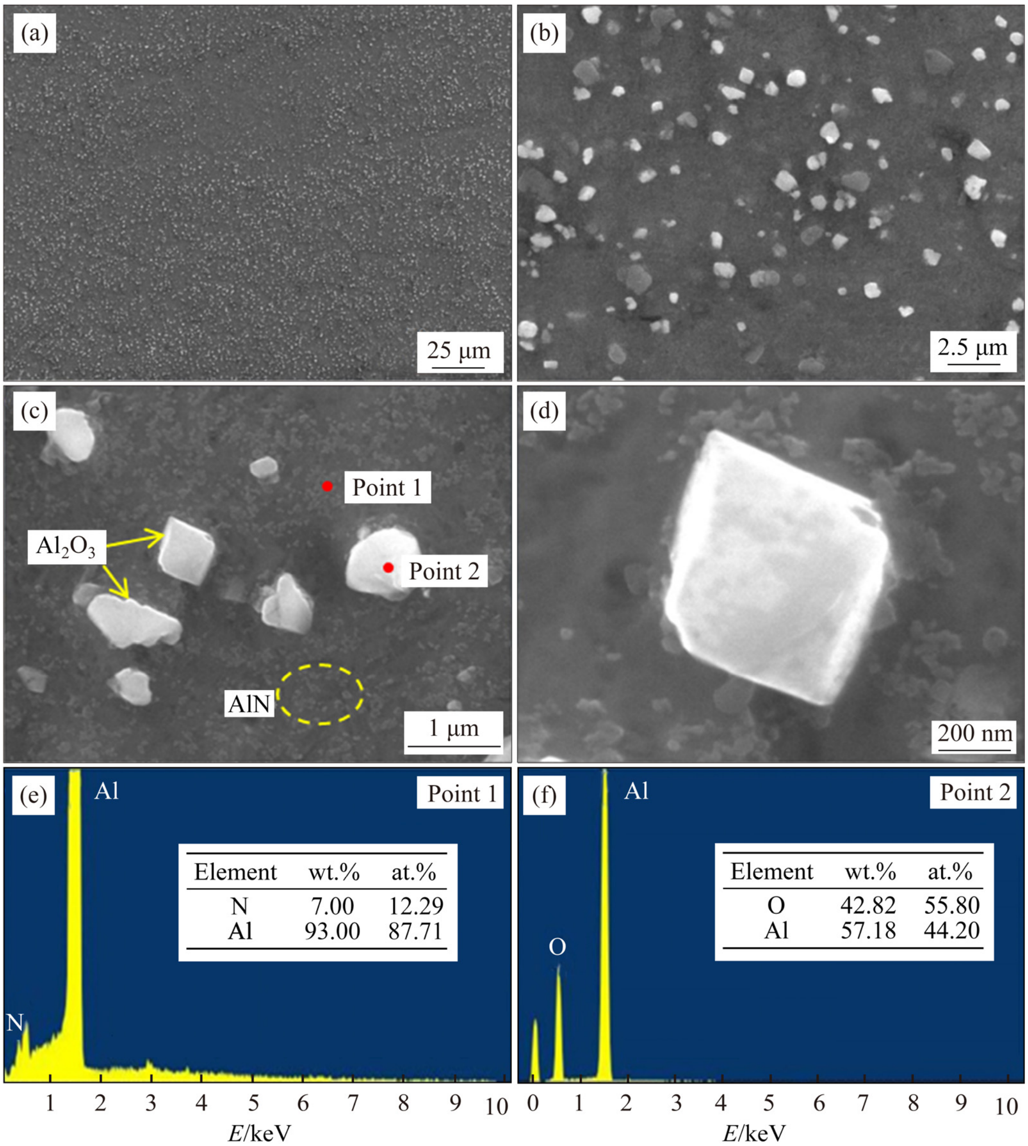

Fig. 4 SEM microstructures and EDS results of T6-treated $(8.2\ AlN + 1\ Al_2O_3)_p$/6061 Al composite: (a) Low magnification; (b−d) High magnification; (e) EDS results of Point 1 in (c); (f) EDS results of Point 2 in (c)

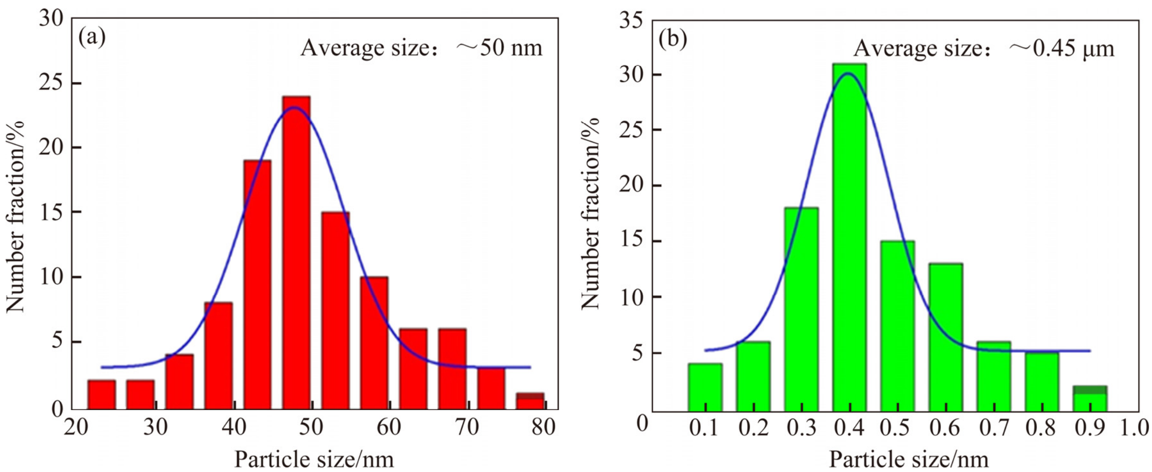

Fig. 5 Statistical size distribution for reinforcement particles: (a) AlN particles with average size of ~50 nm; (b) Al_2O_3 particles with average size of ~0.45 μm

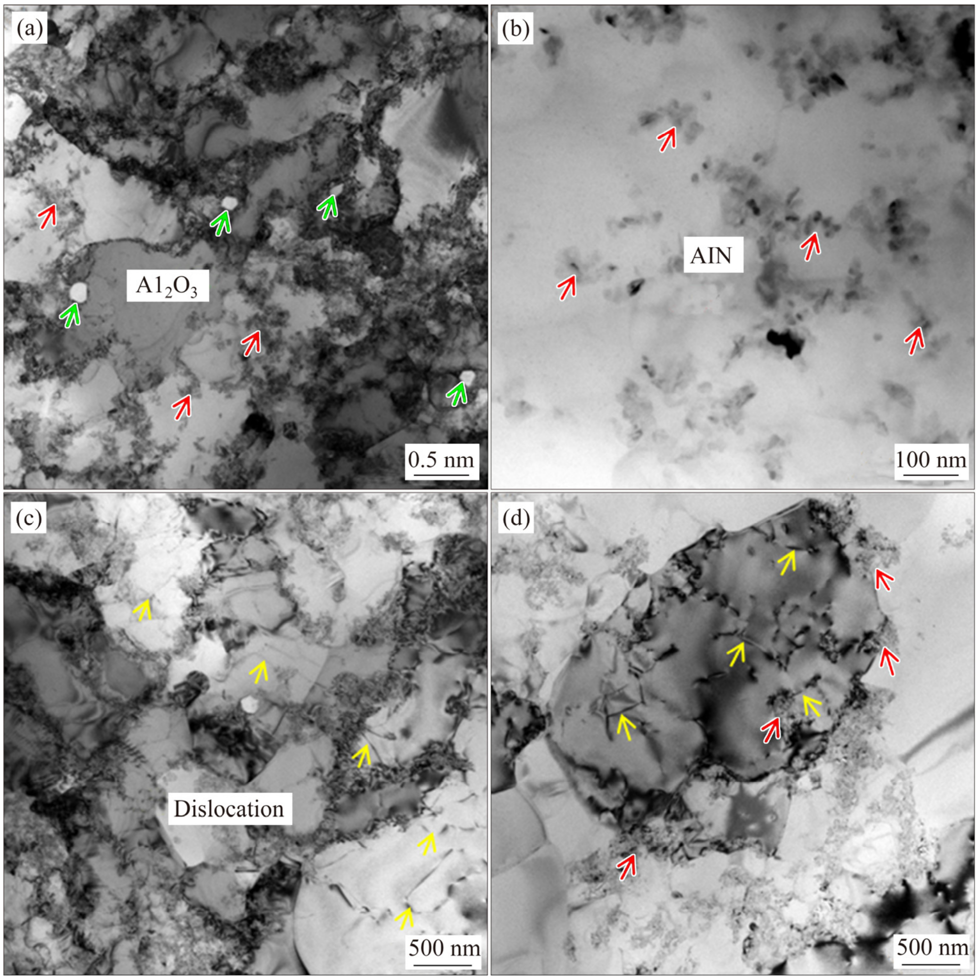

Fig. 6 Typical TEM images of T6-treated (8.2 AlN + 1 Al_2O_3)$_p$/6061 Al composite: (a) Distribution of Al_2O_3 and AlN particles in matrix; (b) Higher magnification TEM image showing dispersive distribution of nano-AlN particles in matrix; (c) Dislocations around particles; (d) Interactions between dislocations and nano-AlN particles both at grain boundaries and in interior of α(Al) grains

extrusion direction, and all the tested samples were taken from the longitudinal section of extrusion rods after T6 heat treatment. As shown in the inverse pole figure (IPF) maps of Figs. 7(a) and (b), the α(Al) grains are stretched along the extrusion direction (ED) on the longitudinal section, and they have some misorientations with each other, which indicates the existence of preferred orientation. According to the pole figures (PFs) of Fig. 7(c), the preferred orientation of the α(Al) grains of 6061 alloy is determined to be both the ⟨100⟩ direction and the ⟨111⟩ direction parallel to the ED. That is to say, both ⟨100⟩ and ⟨111⟩ fiber textures are formed in 6061 alloy. While, for the (8.2 AlN + 1 Al_2O_3)$_p$/6061 Al composite, the preferred orientation of the α(Al) grains has evolved obviously. In detail, the ⟨100⟩ direction of α(Al) grains parallel to ED was weakened and the orientation changed from consistent orientation to random orientation on the longitudinal section. However, the degree of ⟨111⟩ orientation parallel to ED increased and the ⟨111⟩ fiber texture became much stronger, as shown in the PFs of Fig. 7(d). As is known to all, along the ⟨111⟩ preferred orientation, the Al alloy has the highest strength with fcc crystallographic structure. Therefore, the stronger the ⟨111⟩ preferred orientation is, the better the mechanical performance will be.

The distributions of recrystallized grains and the statistic grain size on longitudinal section of the two samples are shown in Fig. 8, respectively. Compared with the 6061 alloy, it can be seen that the fraction of recrystallized grains in the composite decreased from 45% to 6%. Reversely, the fraction

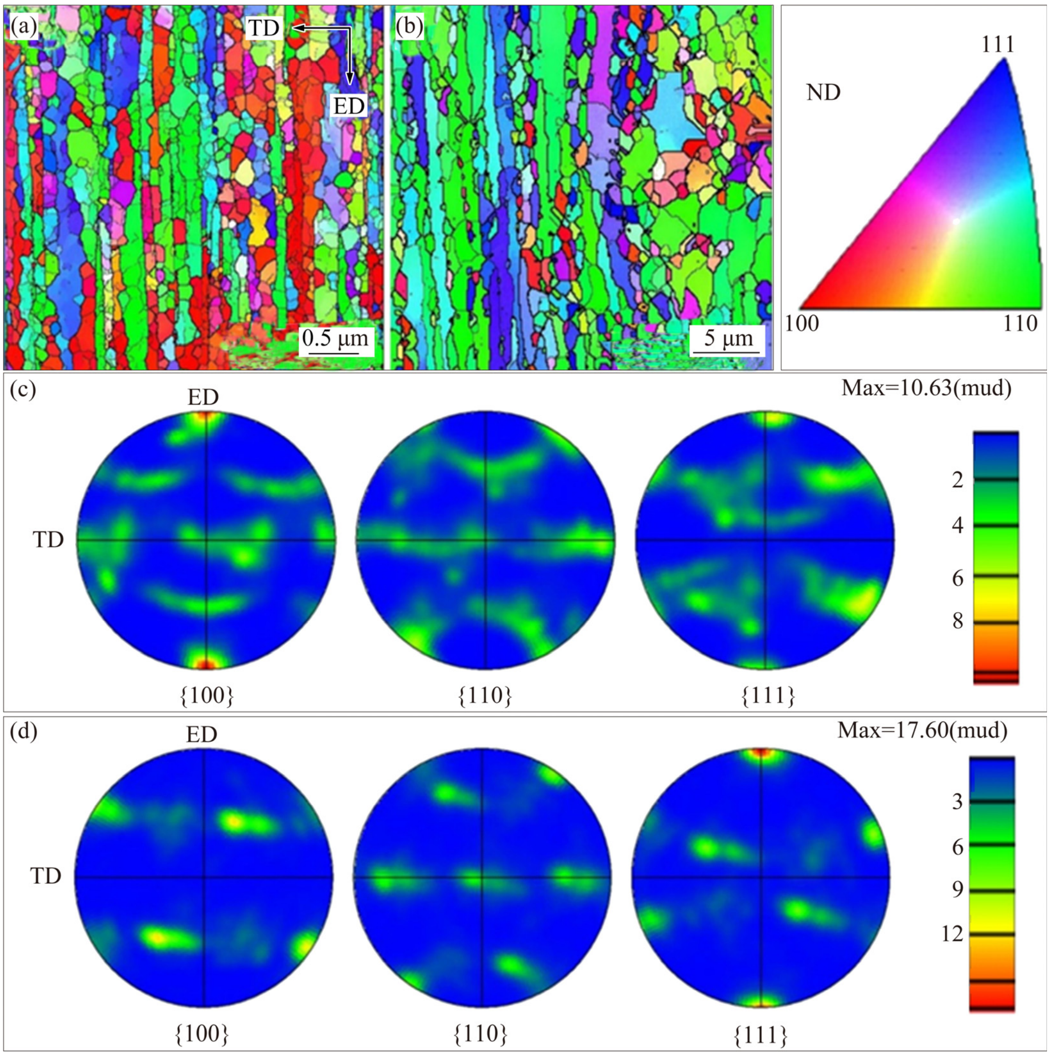

Fig. 7 EBSD analysis results of α(Al) grains along extrusion direction: (a) Inverse pole figure (IPF) map of α(Al) grains of 6061 alloy; (b) IPF map of α(Al) grains of (8.2 AlN + 1 Al_2O_3)$_p$/6061 Al composite; (c) Pole figures (PFs) obtained from (a); (d) PFs obtained from (b) (To easily describe texture, extrusion direction (ED), transverse direction (TD) and normal direction (ND) have been marked in figures)

of substructured grains significantly increased from 46% to 91% in the (8.2 AlN + 1 Al_2O_3)$_p$/6061 Al composite, as shown in Figs. 8(b) and (e), respectively. Besides, the 6061 alloy has an average α(Al) grain size of 21.6 μm, as shown in Fig. 8(c). And the corresponding α(Al) grain size of the (8.2 AlN + 1 Al_2O_3)$_p$/6061 Al composite is shown in Fig. 8(f). Obviously, most of the coarse α(Al) grains are refined significantly and have a much smaller mean size of 1.2 μm than those of the 6061 alloy. According to the above results, it can be concluded that the nano-AlN and submicron-Al_2O_3 particles have a significant refinement effect on the matrix grains of the composite, which is mostly due to the hindered recrystallization and the blocking effect on the migration of grain boundary by the high density of reinforcement particles during the hot extrusion process [23,24].

3.3 Tensile mechanical properties of (8.2 AlN+ 1 Al_2O_3)$_p$/6061 Al composite

The tensile mechanical properties of the 6061 alloy and (8.2 AlN + 1 Al_2O_3)$_p$/6061 Al composite after T6 heat treatment (peak aging) were tested at room temperature and 350 °C in this work. Figure 9(a) depicts the engineering stress−strain curves at room temperature, and the detailed values of ultimate tensile strength (UTS), yield strength (YS) and elongation to failure (EF) are summarized in Table 1. Obviously, when compared with the

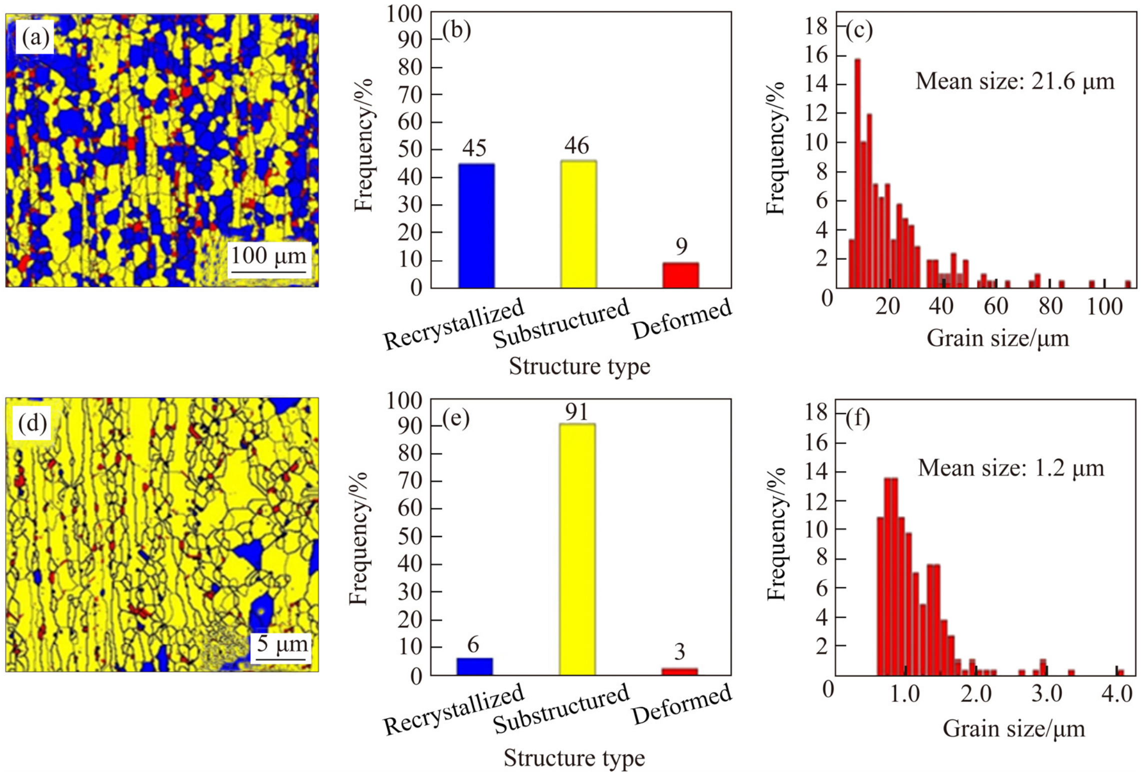

Fig. 8 Recrystallization maps (Recrystallized structures are shown in blue, while substructured and deformed structures in yellow and red, correspondingly) (a, b, d, e) and statistic distribution of α(Al) grain size on longitudinal section (c, f): (a−c) 6061 alloy; (d−f) (8.2 Al N + 1 Al_2O_3)$_p$/6061 Al composite

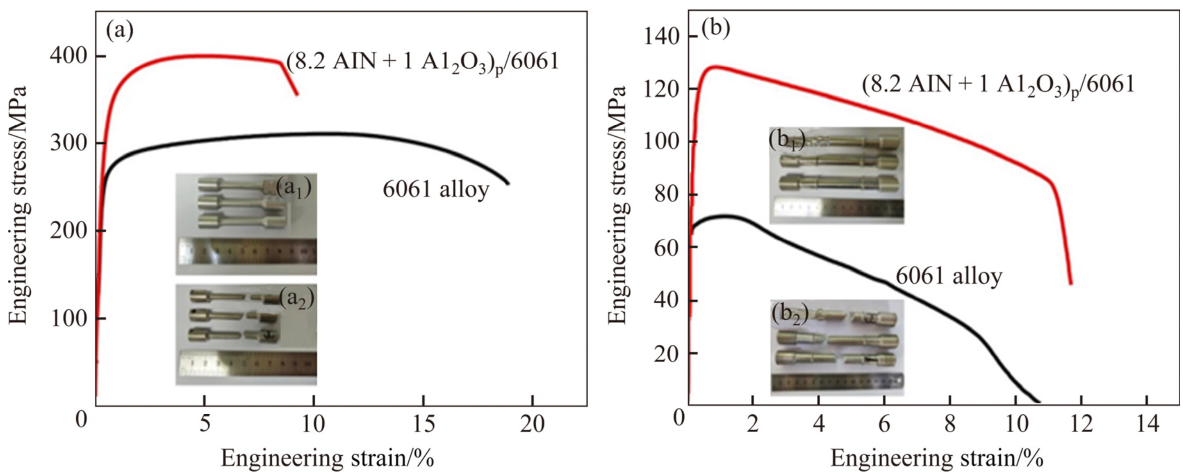

Fig. 9 Engineering strain−stress curves of 6061 alloy and (8.2 AlN + 1 Al_2O_3)$_p$/6061 Al composite after T6 heat treatment (peak aging) tested at room temperature (a) and 350 °C (b) (The inset illustrations show the specimens before (a_1, b_1) and after (a_2, b_2) tensile test)

Table 1 Ultimate tensile strength, yield strength and elongation to failure of T6-treated samples (peak aging) at room temperature and 350 °C

Sample	Room temperature			350 °C		
	UTS/MPa	YS/MPa	EF/%	UTS/MPa	YS/MPa	EF/%
6061 alloy	310±4	265±5	19.0±0.5	72±3	69±2	10.8±0.2
(8.2 AlN + 1 Al_2O_3)$_p$/6061	400±5	320±4	8.6±0.3	128±4	121±3	11.6±0.4

unreinforced 6061 alloy, the tensile strength of the $(8.2\ AlN + 1\ Al_2O_3)_p$/6061 Al composite is significantly improved and the UTS of the T6-treated composite reaches up to 400 MPa, about 29.0% higher than that of the matrix alloy. However, the EF of the composite decreases due to the existence of reinforcement particles.

In order to investigate the high temperature mechanical properties of the composite, tensile tests of the composite at 350 °C were also carried out, and the results are shown in Fig. 9(b) and Table 1. It can be found that the T6-treated $(8.2\ AlN + 1\ Al_2O_3)_p$/6061 Al composite exhibits a high UTS of 128 MPa, which is 56 MPa higher than that of the unreinforced 6061 alloy, indicating the effective strengthening effects of AlN and Al_2O_3 particles at elevated temperature. Meanwhile, one point which needs to mention is that the EF of the T6-treated composite reaches up to 11.6%, which is also slightly better than that of the unreinforced 6061 alloy (10.8%). That is to say, the T6-treated $(8.2\ AlN + 1\ Al_2O_3)_p$/6061 Al composite fabricated in the present work has remarkable tensile mechanical properties at 350 °C.

3.4 Fracture behavior of $(8.2\ AlN + 1\ Al_2O_3)_p$/6061 Al composite

In order to understand the tensile deformation behavior, the fracture of the $(8.2\ AlN + 1\ Al_2O_3)_p$/6061 Al composite after T6 heat treatment was investigated. Figures 10(a) and (c) show the typical fracture morphologies of the $(8.2\ AlN + 1\ Al_2O_3)_p$/6061 Al composite at room temperature. Lots of equiaxed dimples with different sizes on the tensile fracture can be observed, indicating the typical plastic fracture feature. At a higher magnification as shown in Fig. 10(c), some AlN particles can be seen at the bottom of the dimples. However, compared with room temperature, the fracture characteristic of $(8.2\ AlN + 1\ Al_2O_3)_p$/6061 Al composite deformed at 350 °C is quite different. As shown in Fig. 10(b), large number of dimples on the fracture surface are much larger and deeper, which is in accordance with the higher ductility at 350 °C. Moreover, at the higher magnification in Fig. 10(d), it is noted that there are large number of nano-AlN particles exposed at the bottom of the dimples as marked by red arrows, indicating that rapid softening of the matrix occurs at 350 °C. At the same time, some submicron-Al_2O_3 particles (marked by green arrows) are detected on the fracture surface. This also indicates that a certain strengthening effect of load-transfer by reinforcement particles occurred during the deformation process.

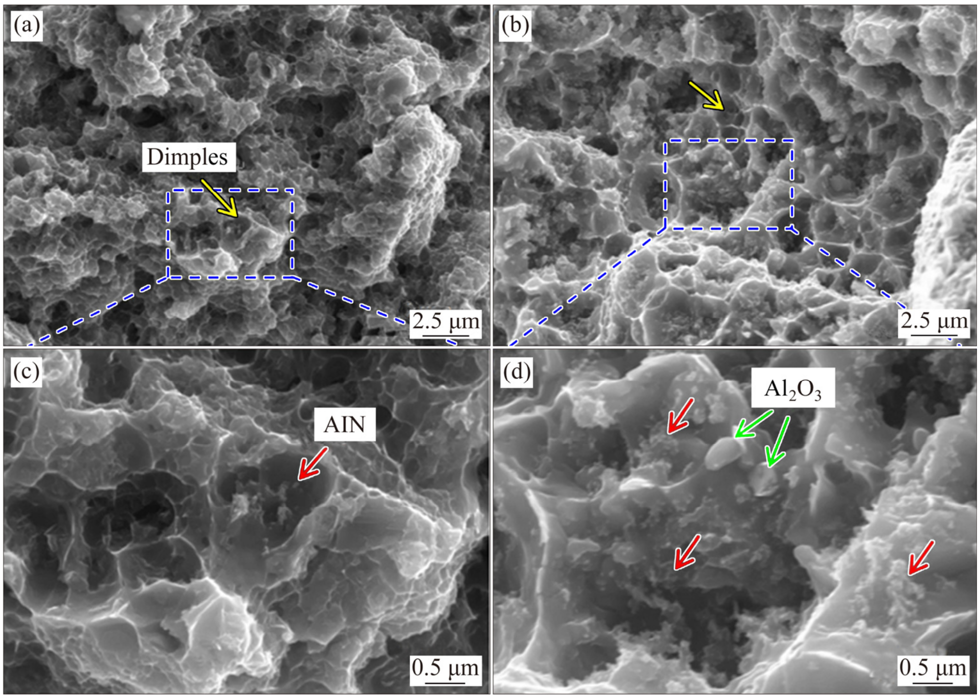

Fig. 10 Tensile fracture morphologies of $(8.2\ AlN + 1\ Al_2O_3)_p$/6061 Al composite after T6 heat treatment showing dimples and reinforcement particles on fracture surfaces at room temperature (a, c) and 350 °C (b, d)

4 Discussion

4.1 Enhanced aging kinetics in (8.2 AlN + 1 Al_2O_3)$_p$/6061 Al composite

A large number of defects and interfaces introduced by the nano-AlN and submicron-Al_2O_3 particles are supposed to have a significant effect on the aging behavior. As shown in Fig. 6(c), high density dislocations can be seen around the reinforcement particles in the composite. Furthermore, Fig. 11 shows the geometrically necessary dislocation (GND) densities in the α(Al) grains which were calculated by EBSD analyses and the color label represents GND density variation in the map, i.e. the red corresponds to the higher dislocation density values, whereas the blue is associated with the lower dislocation density values. Specifically, the average GND densities of the 6061 alloy and (8.2 AlN + 1 Al_2O_3)$_p$/6061 Al composite are calculated to be 7.9×10^{13}/m^2 and 6.4×10^{14}/m^2, respectively. As evident from the above results, the average dislocation density in the composite is significantly higher than that in the 6061 alloy. During the heat treatment process, these extra quantities of dislocations in the composite not only served as the additional heterogeneous nucleation sites for the formation of Guinier–Preston (GP) zones and/or early precipitate clusters, but also increased the solute diffusivity significantly in the composite and then boosted the growth rate of precipitates [25]. As a result, the aging kinetics process of the composite is accelerated to a large extent.

4.2 Strengthening mechanism at room temperature

As mentioned above, it is indicated that the homogeneous distribution of nano-AlN and submicron-Al_2O_3 particles played an effective

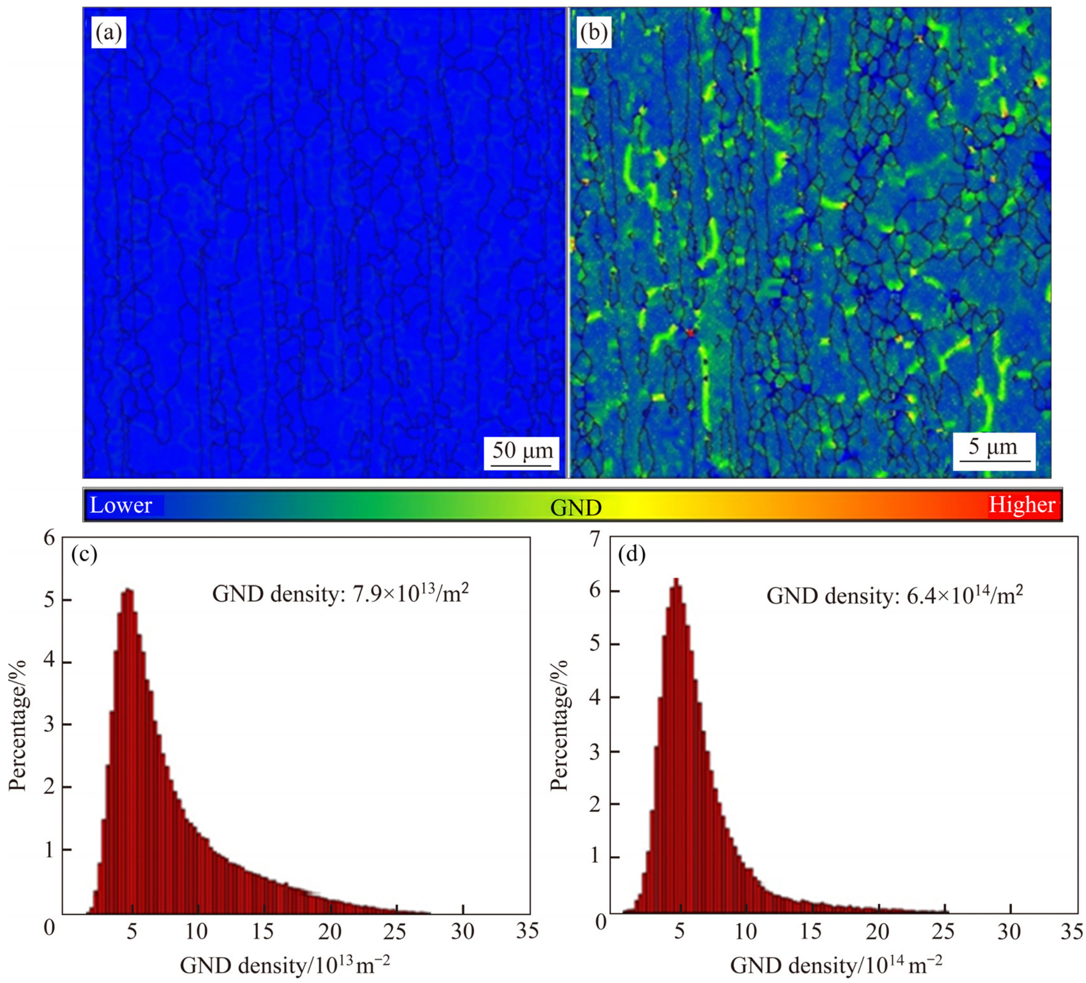

Fig. 11 Geometrically necessary dislocation (GND) densities calculated by EBSD analysis: (a, c) 6061 alloy; (b, d) (8.2 AlN + 1 Al_2O_3)$_p$/6061 Al composite

strengthening effect on the 6061 Al matrix composite. According to the strengthening mechanisms for composite, the yield strength of the composite can be expressed as [26]

$$\sigma_{yc}=\sigma_{ym}+\Delta\sigma_{AlN}+\Delta\sigma_{Al_2O_3} \quad (1)$$

where σ_{yc} is the yield strength of the composite, σ_{ym} is the yield strength of Al matrix, $\Delta\sigma_{AlN}$ is the strength increase contributed by the AlN particles, and $\Delta\sigma_{Al_2O_3}$ is the strength increase contributed by the Al_2O_3 particles.

The yield strength of Al matrix could be estimated as follows [27]:

$$\sigma_{ym}=\sigma_0+\frac{K_{HP}}{\sqrt{D}} \quad (2)$$

where σ_0 is the friction stress (20 MPa), D is the average grain size of α(Al) (1.2 μm in this study), and K_{HP} is the Hall–Petch slope (40 MPa·$\mu m^{1/2}$ for Al).

The strengthening effect of AlN particles comes from: (1) secondary strengthening by dislocation accumulation, including Orowan strengthening ($\Delta\sigma_{Or}$) and GND strengthening ($\Delta\sigma_{GND}$), and (2) strengthening by load-transfer ($\Delta\sigma_{L\text{-}T}$) [28]. Therefore,

$$\Delta\sigma_{AlN}=\Delta\sigma_{Or}+\Delta\sigma_{GND}+\Delta\sigma_{L\text{-}T} \quad (3)$$

For particle reinforced metal matrix composites, Orowan strengthening is one of the most important strengthening mechanisms. According to Ref. [29], the Orowan strengthening ($\Delta\sigma_{Or}$) can be expressed as

$$\Delta\sigma_{Or}=\frac{MGb}{2.36\pi}\ln\left(\frac{d}{2b}\right)\frac{1}{\lambda-d} \quad (4)$$

where M is the Taylor factor (taken as 3.06 for Al), G(=25.4 GPa) is the shear modulus of Al, b(=0.286 nm) is the magnitude of Burger vector of Al, d is the average particle diameter, and λ is the average inter-particle spacing [30].

The yield strength increase caused by GND strengthening ($\Delta\sigma_{GND}$) can be calculated according to Ref. [31]:

$$\Delta\sigma_{GND}=\alpha Gb\sqrt{\frac{8V_p\varepsilon_y}{bB}} \quad (5)$$

where α is the constant equal to 1.25, B is the diameter of the prismatic dislocation loop around the particles (approximate to the average diameter of reinforcement particles), V_p is the volume fraction of reinforcement particles (V_p is 7% and 0.7% for AlN and Al_2O_3 particles in this study, respectively), and ε_y is the yielding strain (value of 0.2%).

Owing to the transfer of tensile stress from matrix to the reinforcements, the strengthening by load-transfer ($\Delta\sigma_{L\text{-}T}$) can be calculated as [32]

$$\Delta\sigma_{L\text{-}T}=0.5V_p\sigma_{ym} \quad (6)$$

Similarly, for Al_2O_3 particles, the yield strength increase caused by Orowan, GND and load-transfer strengthening are also calculated by using Eqs. (4−6), respectively. And the calculated results and deviations are summarized in Table 2.

From Table 2, it can be seen that the prediction of yield strength of the composite was relatively accurate with a small deviation of only 7.8 MPa, which indicates there is a good agreement between the calculated values and experimental data at room temperature. Meanwhile, it can be seen that the strengthening effect coming from nano-AlN particles makes up the very large proportion of yield strength. In addition, the Orowan strengthening is the dominant one.

4.3 Strengthening mechanism at elevated temperature

It is well known that under high temperature, the grain boundaries would soften and slide easily. That is to say, when the tensile temperature increased up to 350 °C, the strength of Al matrix alloys deteriorated and grain boundary sliding occurred during the deformation. So, the high strength of grain boundary decreased significantly at high temperature of 350 °C, and the grain boundaries cannot provide strengthening effect any longer as they do at room temperature. However,

Table 2 Calculated values of yield strength of (8.2 AlN + 1 Al_2O_3)$_p$/6061 Al composite at room temperature

$\Delta\sigma_{ym}$/MPa	AlN			Al_2O_3			Combined prediction/MPa	Deviation/MPa
	$\Delta\sigma_{Or}$/MPa	$\Delta\sigma_{GND}$/MPa	$\Delta\sigma_{L\text{-}T}$/MPa	$\Delta\sigma_{Or}$/MPa	$\Delta\sigma_{GND}$/MPa	$\Delta\sigma_{L\text{-}T}$/MPa		
57	156	80	2	9	8	0.2	312.2	7.8

fine ceramic particles pin at the grain boundaries and hinder the grain boundary sliding at high temperature, which is an effective strategy to improve the stability of the grain boundary at high temperatures [33]. In this work, as indicated in Fig. 6(a), the nano-AlN particles located at the α(Al) grain boundaries play a significant effect on pinning and hindering grain boundary sliding and then improving the stability of them, consequently, the high temperature strength of the composite at 350 °C has been significantly improved.

What's more, dislocations tended to surmount the particles by climbing rather than bypassing at high temperatures [34,35]. For particle-reinforced metal matrix composites, the maximum stress resisting dislocation climb occurs either on the arrival side or on the departure side, resulting in a barrier for dislocation climbing, or a detachment barrier, respectively [36]. In the unreinforced matrix alloy, dislocations could not form pile-ups and most of them annihilated at the grain boundaries. While, for the composite, intragranular nano-AlN particles act as obstacles interacting with dislocations to impede their motion and make them harder for climbing over, so more energy is needed for accommodating to maintain further deformation, resulting in higher tensile strength to a certain extent. And also, during the deformation process at 350 °C, a microstructure of low angle boundary, i.e. subgrain boundary, developed, which resulted from the dislocations motion and interaction with nano-AlN particles, as shown in Fig. 12.

Based on the above results and analyses, a schematic illustration can be summarized to generalize the high-temperature tensile behavior of the composite, as shown in Fig. 13. At high temperature of 350 °C, nano-AlN particles play an extremely important role in the tensile strength of

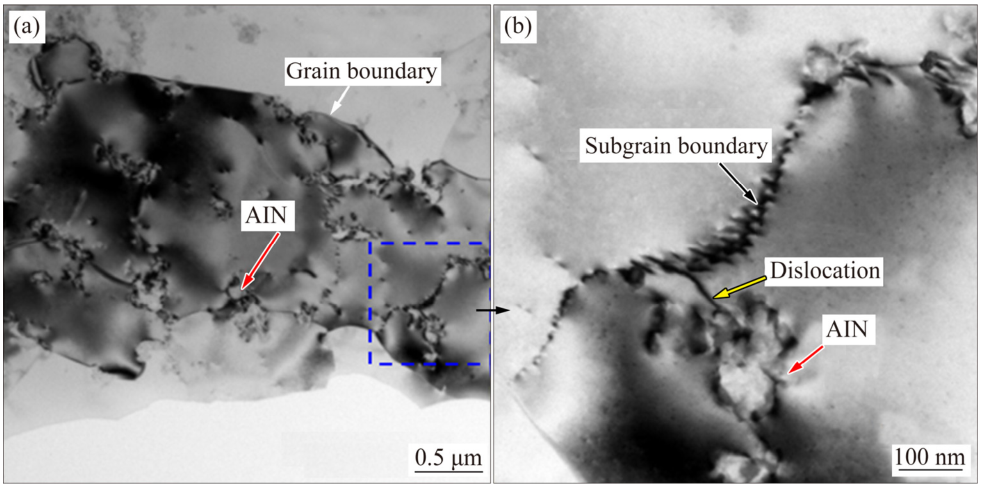

Fig. 12 TEM images of composite after tensile test at 350 °C and subgrain boundary developed by dislocations motion and interaction with nano-AlN particles

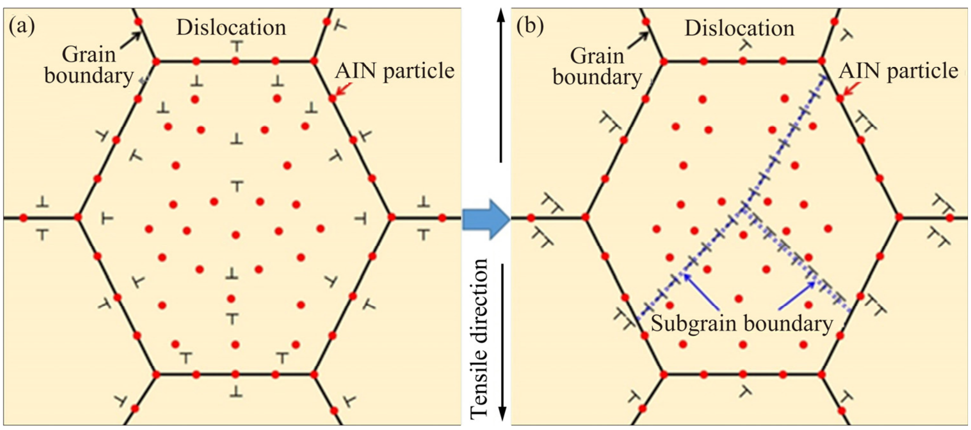

Fig. 13 Schematic illustration showing strengthening of nano-AlN particles in (8.2 AlN + 1 Al_2O_3)$_p$/6061 Al composite during tensile deformation at high temperature: (a) Homogenous distribution of intragranular and intergranular nano-AlN particles in α(Al) matrix before tensile deformation; (b) Subgrain boundary developed during deformation process

the composite. Not only can the intragranular nano-AlN particles pin dislocation motion, but, more importantly, nano-AlN particles located exactly at the grain boundaries are more effective in strengthening the Al matrix by stabilizing the grain boundaries and preventing dislocations from annihilating at elevated temperatures. Therefore, making nano-AlN particles distributed at the grain boundaries is an effective strategy to improve the high-temperature strength.

5 Conclusions

(1) The aging kinetics of the 6061 Al matrix composite has been accelerated by the AlN and Al_2O_3 particles. Compared with the age hardening curves of the composite and the matrix alloy, the time to peak aging at 175 °C for the composite is reduced from 8 to 6 h.

(2) According to the EBSD analyses, the ⟨111⟩ fiber texture is formed in the 6061 Al matrix composite. As the reinforcement particles have a significant refinement effect on α(Al) grains, the mean α(Al) grain size of the composite is 1.2 μm, which is much smaller than that of the unreinforced 6061 Al alloy (21.6 μm).

(3) Nano-AlN particles exhibit significant strengthening effects on the composite at both room temperature and 350 °C. At room temperature, the UTS of the T6-treated composite reaches up to 400 MPa. At 350 °C, the composite not only has high YS of 121 MPa and UTS of 128 MPa, but also exhibits a larger elongation of 11.6% than that of the unreinforced matrix alloy (10.8%).

(4) At room temperature, the strengthening mechanisms of nano-AlN and submicron-Al_2O_3 particles include Orowan strengthening, geometrically necessary dislocation strengthening and load-transfer strengthening. Among them, the Orowan strengthening effect coming from nano-AlN particles is confirmed to be the dominant one.

(5) It was proven that the intergranular nano-AlN particles contributed to the high-temperature (up to 350 °C) tensile strength significantly. At elevated temperature, intergranular nano-AlN particles enhanced the stability of the grain boundaries and intragranular nano-AlN particles hindered dislocation motion during the deformation process, resulting in the fact that the composite exhibited a high tensile strength.

Acknowledgments

This work was financially supported by the Key Program of National Natural Science Foundation of China (No. 51731007), the National Natural Science Foundation of China (No. 52071179), and the Fundamental Research Funds for the Central Universities (No. 30920021160).

References

[1] WANG Pei, ECKERT J, PRASHANTH K G, WU Ming-wei, KABAN I, XI Li-xia, SCUDINO S. A review of particulate-reinforced aluminum matrix composites fabricated by selective laser melting [J]. Transactions of Nonferrous Metals Society of China, 2020, 30: 2001−2034.

[2] NIE Jin-feng, CHEN Yu-yao, CHEN Xiang, LIU Xiang-fa, LIU Gui-liang, ZHAO Yong-hao, ZHU Yun-tian. Stiff, strong and ductile heterostructured aluminum composites reinforced with oriented nanoplatelets [J]. Scripta Materialia, 2020, 189: 140−144.

[3] SAESSI M, ALIZADEH A, ABDOLLAHI A. Wear behavior and dry sliding tribological properties of ultra-fine grained Al5083 alloy and boron carbide-reinforced Al5083-based composite at room and elevated temperatures [J]. Transactions of Nonferrous Metals Society of China, 2021, 31: 74−91.

[4] GUDLUR P, FORNESS A, LENTZ J, RADOVIC M, MULIANA A. Thermal and mechanical properties of Al/Al_2O_3 composites at elevated temperatures [J]. Materials Science and Engineering A, 2012, 531: 18−27.

[5] LIU Xiao-yan, PAN Qing-lin, ZHENG Li-yun, FU Quan-rong, GAO Fei, LI Mei-xia, BAI Yong-mei. Effect of aging temper on the thermal stability of Al–Cu–Mg–Ag heat-resistant alloy [J]. Materials & Design, 2013, 46: 360−365.

[6] TAO Jia-shen, ZHANG Liang, WU Guo-hua, CHEN An-tao, ZHANG Xiao-long, SHI Chun-chang. Effect of heat treatment on the microstructure and mechanical properties of extruded Al−4Cu−1Li−0.4Mg−0.4Ag−0.18Zr alloy [J]. Materials Science and Engineering A, 2018, 717: 11−19.

[7] YUE H Y, SONG S S, WANG B, GAO X, ZHANG S L, YAO L H, LIN X Y, GUAN E H, ZHANG H J, GUO E J. Effects of whisker surface treatment on microstructures, tensile properties and aging behaviors of $Al_{18}B_4O_{33w}$/6061Al composites [J]. Journal of Alloys and Compounds, 2017, 697: 11−18.

[8] GAO Guan-jun, HE Chen, LI Yong, LI Jia-dong, WANG Zhao-dong, MISRA R D K. Influence of different solution methods on microstructure, precipitation behavior and mechanical properties of Al−Mg−Si alloy [J]. Transactions of Nonferrous Metals Society of China, 2018, 28: 839−847.

[9] TORBATI-SARRAF H, TORBATI-SARRAF S A, CHAWLA N, POURSAEE A. A comparative study of corrosion behavior of an additively manufactured Al-6061 RAM2 with extruded Al-6061 T6 [J]. Corrosion Science, 2020, 174: 108838.

[10] BI Jiang, ZHAO Chang-cai, DU Bing, GUO Qin-bo, DONG Guo-jiang. Formability and strengthening mechanism of AA6061 tubular components under solid granule medium internal high pressure forming [J]. Transactions of Nonferrous Metals Society of China, 2018, 28: 226−234.

[11] UDDIN S Z, MURR L E, TERRAZAS C A, MORTON P, ROBERSON D A, WICKER R B. Processing and characterization of crack-free aluminum 6061 using high-temperature heating in laser powder bed fusion additive manufacturing [J]. Additive Manufacturing, 2018, 22: 405−415.

[12] KALINENKO A, KIM K, VYSOTSKIY I, ZUIKO I, MALOPHEYEV S, MIRONOV S, KAIBYSHEV R. Microstructure-strength relationship in friction-stir welded 6061-T6 aluminum alloy [J]. Materials Science and Engineering A, 2020, 793: 139858.

[13] SEIDMAN D N, MARQUIS E A, DUNAND D C. Precipitation strengthening at ambient and elevated temperatures of heat-treatable Al(Sc) alloys [J]. Acta Materialia, 2002, 50: 4021−4035.

[14] MAKINENI S K, SUGATHAN S, MEHER S, BANERJEE R, BHATTACHARYA S, KUMAR S, CHATTOPADHYAY K. Enhancing elevated temperature strength of copper containing aluminium alloys by forming $L1_2$ Al_3Zr precipitates and nucleating θ'' precipitates on them [J]. Scientific Reports, 2017, 7: 11154.

[15] POLMEAR I J, COUPER M J. Design and development of an experimental wrought aluminum alloy for use at elevated temperatures [J]. Metallurgical Transactions A, 1988, 19: 1027−1035.

[16] TIAN Wei-si, ZHAO Qing-long, ZHANG Qing-quan, QIU Feng, JIANG Qi-chuan. Simultaneously increasing the high-temperature tensile strength and ductility of nano-sized TiC_p reinforced Al−Cu matrix composites [J]. Materials Science and Engineering A, 2018, 717: 105−112.

[17] QIAN Feng, JIN Shen-bao, SHA Gang, LI Yan-jun. Enhanced dispersoid precipitation and dispersion strengthening in an Al alloy by microalloying with Cd [J]. Acta Materialia, 2018, 157: 114−125.

[18] GAO Yu-yang, QIU Feng, GENG Run, CHU Jian-ge, ZHAO Qing-long, JIANG Qi-chuan. Effects of nanosized TiC_p dispersion on the high-temperature tensile strength and ductility of in situ TiC_p/Al−Cu−Mg−Si nanocomposites [J]. Journal of Alloys and Compounds, 2019, 774: 425−433.

[19] NIE Jin-feng, LU Feng-hua, HUANG Zhao-wen, MA Xia, ZHOU Hao, CHEN Cai, CHEN Xiang, YANG Hua-bing, CAO Yang, LIU Xiang-fa, ZHAO Yong-hao, ZHU Yun-tian. Improving the high-temperature ductility of Al composites by tailoring the nanoparticle network [J]. Materialia, 2020, 9: 100523.

[20] KUMAR S, SARMA V S, MURTY B S. High temperature wear behavior of Al−4Cu−TiB_2 in situ composites [J]. Wear, 2010, 268: 1266−1274.

[21] REDDY M P, UBAID F, SHAKOOR R A, PARANDE G, MANAKARI V, MOHAMED A M A, GUPTA M. Effect of reinforcement concentration on the properties of hot extruded Al−Al_2O_3 composites synthesized through microwave sintering process [J]. Materials Science and Engineering A, 2017, 696: 60−69.

[22] XIE Ke-wei, NIE Jin-feng, MA Xia, LIU Xiang-fa. Increasing the ductility of heat-resistant AlN_p/Al composites by submicron Al_2O_3 particles [J]. Materials Characterization, 2020, 170: 110672.

[23] ALIZADEH M. Strengthening mechanisms in particulate Al/B_4C composites produced by repeated roll bonding process [J]. Journal of Alloys and Compounds, 2011, 509: 2243−2247.

[24] WANG Lei, QIU Feng, ZHAO Qing-long, WANG Hui-yuan, JIANG Qi-chuan. Simultaneously increasing the elevated-temperature tensile strength and plasticity of in situ nano-sized TiC_x/Al−Cu−Mg composites [J]. Materials Characterization, 2017, 125: 7−12.

[25] FALLAH V, KORINEK A, OFORI-OPOKU N, RAEISINIA B, GALLERNEAULT M, PROVATAS N, ESMAEILI S. Atomic-scale pathway of early-stage precipitation in Al−Mg−Si alloys [J]. Acta Materialia, 2015, 82: 457−467.

[26] KAI X Z, LI Z Q, FAN G L, GUO Q, XIONG D B, ZHANG W L, SU Y S, LU W J, MOON W J, ZHANG D. Enhanced strength and ductility in particulate-reinforced aluminum matrix composites fabricated by flake powder metallurgy [J]. Materials Science and Engineering A, 2013, 587: 46−53.

[27] REIHANIAN M, EBRAHIMI R, TSUJI N, MOSHKSAR M M. Analysis of the mechanical properties and deformation behavior of nanostructured commercially pure Al processed by equal channel angular pressing (ECAP) [J]. Materials Science and Engineering A, 2008, 473: 189−194.

[28] CHAWLA N, SHEN Yu-lin. Mechanical behavior of particle reinforced metal matrix composites [J]. Advanced Engineering Materials, 2001, 3: 357−370.

[29] MUÑOZ-MORRIS M A, OCA C G, MORRIS D G. An analysis of strengthening mechanisms in a mechanically alloyed, oxide dispersion strengthened iron aluminide intermetallic [J]. Acta Materialia, 2002, 50: 2825−2836.

[30] SHEN Jiang-hua, YIN Wei-hua, WEI Qiu-ming, LI Yu-long, LIU Jin-ling, AN Li-nan. Effect of ceramic nanoparticle reinforcements on the quasistatic and dynamic mechanical properties of magnesium-based metal matrix composites [J]. Journal of Materials Research, 2013, 28: 1835−1852.

[31] TANG Fei, ANDERSON I E, GNAUPEL-HEROLD T, PRASK H. Pure Al matrix composites produced by vacuum hot pressing: Tensile properties and strengthening mechanisms [J]. Materials Science and Engineering A, 2004, 383: 362−373.

[32] ZHANG Z, CHEN D L. Consideration of Orowan strengthening effect in particulate-reinforced metal matrix nanocomposites: A model for predicting their yield strength [J]. Scripta Materialia, 2006, 54: 1321−1326.

[33] POLETTI C, BALOG M, SIMANCIK F, DEGISCHER H P. High-temperature strength of compacted sub-micrometer aluminium powder [J]. Acta Materialia, 2010, 58: 3781−3789.

[34] ZHU S M, TJONG S C, LAI J K L. Creep behavior of a β'(NiAl) precipitation strengthened ferritic Fe−Cr−Ni−Al alloy [J]. Acta Materialia, 1998, 46: 2969−2976.

[35] QIN J, ZHANG Z, CHEN X G. Mechanical properties and strengthening mechanisms of Al−15 pct B_4C composites

with Sc and Zr at elevated temperatures [J]. Metallurgical and Materials Transactions A, 2016, 47: 4694−4708.
[36] ARZT E, WILKINSON D S. Threshold stresses for dislocation climb over hard particles: The effect of an attractive interaction [J]. Acta Metallurgica, 1986, 34: 1893−1898.

利用纳米 AlN 和亚微米 Al_2O_3 双相颗粒提高 6061 铝基复合材料的高温强度

谢可伟[1]，聂金凤[2]，胡恺琪[1]，马 霞[3]，刘相法[1]

1. 山东大学 材料液固结构演变与加工教育部重点实验室，济南 250061；
2. 南京理工大学 材料科学与工程学院 纳米异构材料中心，南京 210094；
3. 山东理工大学 机械工程学院，淄博 255000

摘 要：为了提高 6061 铝基复合材料的高温性能，利用纳米 AlN 和亚微米 Al_2O_3 颗粒对其进行强化。由 SEM 和 TEM 表征结果可知，纳米 AlN 和亚微米 Al_2O_3 颗粒均弥散分布于铝基体中。布氏硬度测试结果表明，与传统 6061 铝合金不同，增强体颗粒明显加快了复合材料的时效动力学。经 T6 热处理的复合材料具有优异的室温和高温拉伸性能。特别是在 350 ℃时，T6 态的复合材料不仅具有 121 MPa 的屈服强度和 128 MPa 的抗拉强度，而且其伸长率高达 11.6%。此外，还详细讨论纳米 AlN 和亚微米 Al_2O_3 颗粒的强化机制。

关键词：6061 铝基复合材料；纳米 AlN 颗粒；亚微米 Al_2O_3 颗粒；高温强度

(Edited by Wei-ping CHEN)